Artificial SA-I and RA-I Afferents for Tactile Sensing of Ridges and Gratings

Nicholas Pestell, Thom Griffith and Nathan F. Lepora

Department of Engineering Mathematics and Bristol Robotics Laboratory,
University of Bristol, BS8 1QU, UK
e-mail: n.pestell@bristol.ac.uk

July 19, 2021

Abstract

For robot touch to converge with the human sense of touch, artificial transduction should involve biologically-plausible population codes analogous to those of natural afferents. Using a biomimetic tactile sensor with 3d-printed skin based on the dermal-epidermal boundary, we propose two novel feature sets to mimic slowly-adapting SA-I and rapidly-adapting RA-I type-I tactile mechanoreceptor function. Their plausibility is tested with three classic experiments from the study of natural touch: impingement on a flat plate to probe adaptation and spatial modulation; stimulation by spatially-complex ridged stimuli to probe single afferent responses; and perception of grating orientation to probe the population response. Our results show a match between artificial and natural afferent responses in their sensitivity to edges and gaps; likewise, the human and robot psychometric functions match for grating orientation. These findings are of benefit to robot manipulation, prosthetics and the neurophysiology of touch.

1 Introduction

The fields of neuroscience and robotics are converging as machines approach animals in their capabilities [1, 2]. Within the somatosensory modalities including touch, a natural convergence is around the engineering of biologically-plausible artificial tactile sensory systems [3, 4]. A biomimetic tactile fingertip or skin can inform about the neurophysiology of human touch [5, 6, 7], lead to improved contact sensing for dexterous robots [8, 9, 10], and could enable neuroprosthetics to restore a sense of touch in amputees [11, 12].

How stimuli are represented (coded) in the peripheral nervous system is important to the field of neuroscience. Within the sense of touch, this includes: *(i)* the dynamics of local skin tissue to which individual receptive units respond; *(ii)* how individual afferent nerve fibres represent these dynamics when stimulated; and *(iii)* how the population of afferents represents the spatial and temporal aspects of the tactile stimulation. Here we propose that, for spatially-detailed static stimuli, the TacTip biomimetic tactile sensor [13, 9] provides a suitable artificial analogue for all three aspects of this process.

Our proposition is underpinned by two positions regarding peripheral neural codes in natural touch. First, in many scenarios, such as those in the present study, spike rate of individual natural afferents may be a suitable metric to model artificial tactile channels because of its correlation with external stimuli [14]. There is a body of evidence which supports this position for touch [15, 16, 17, 18]. Second, population codes, more specifically, the spatial patterns of firing rates across afferent populations, is essential and is the primary abstract coding scheme for many spatially-detailed static stimuli in natural touch. Again, there is a body of evidence that supports this position [19, 20, 18, 15].

Specifically, the shallow layers of skin on the fingertip are structured to sense touch via the deformation of its surface. These upper layers comprise an outer *epidermis* over an inner *papillar dermis*, which interdigitate in a mesh of dermal *papillae* and epidermal *intermediate ridges* (Figure 1D). This 3D structure transmits shear and normal deformation of the skin surface into the displacement of two shallow populations of slowly adapting (SA-I) and rapidly adapting (RA-I) sensory mechanoreceptors near the dermal-epidermal interface. Thus, the dermal papillae and intermediate ridges may act as a mechanical amplifier [21] of skin deformation into slow (sustained contact) and fast (changing contact) mechanoreceptor activity.

The TacTip design is based on the shallow layers of glabrous skin [13, 9]. It has an outer biomimetic epidermis made from a rubber-like material over a soft inner biomimetic dermis made from an elastomer gel (Figure 1E). These two materials interdigitate in a mesh of biomimetic intermediate ridges and dermal papillae, comprising stiff inner nodular pins that extend under the biomimetic epidermis into the soft gel. This structure amplifies surface deformation of the skin into lateral movement of visible markers on the pin tips. Markers are imaged optically by a USB camera and thus raw tactile data is available as images of the shear-strain profile within the gel.

We propose two novel feature sets derived from the tactile images to mimic SA-I and RA-I afferents in humans. Natural SA-I firing rates are modelled by the marker displacements from their at-rest position and natural RA-I firing rates are modelled by the marker speeds. The basic rationale behind these models is that marker displacement is sustained with a static stimulus and marker velocity is non-zero only when the stimulus changes, *e.g.* presented or removed. Markers are arranged in a 19×19 square array ($\sim500\,\mathrm{mm}^2$). Thus there are 361 artificial SA-I and RA-I afferents, with a density of $\sim70\,\mathrm{cm}^{-2}$ ($\sim1.2\,\mathrm{mm}$ separation) which is approximately half the innervation density of type-I afferents in the human fingertip [22, 23].

To examine this proposal, we perform two studies of the response of artificial afferents to a normal force stimulation (Experiments 1a) and complex spatial stimuli (Experiment 1b), followed by a perceptual experiment for assessing the validity of artificial population codes from these artificial afferents (Experiment 2). Experiments 1b and 2 mirror two classic studies of human and primate tactile population coding by Phillips and Johnson (1981) [16, 15]. We compare the specific dynamic

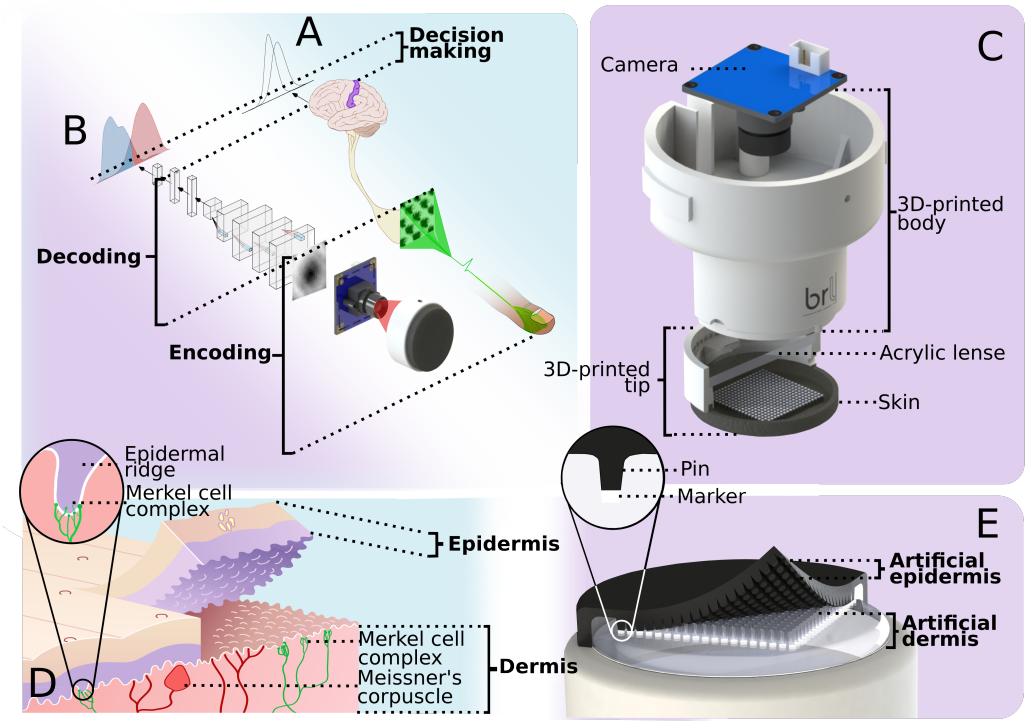

Figure 1: (**A**,**B**) Perceptual pipelines of human and robot touch. Spatial encoding involves representing the stimulus in the spatial modulation of firing rates in populations of natural and artificial type-I afferents. In human touch, decoding is performed in the somatosensory cortex (highlighted on the brain image). Here, in robot touch, an artificial decoder is constructed from a CNN. Decision making is depicted in a SDT framework, where the decoded decision variable is compared to a criterion. (**C**) Exploded view of the BRL TacTip showing 3d-printed body and tip. (**D**) Diagram of human (hairless) skin, *e.g.* the fingertip, showing the stiff epidermis (outer skin) with epidermal ridges protruding into the softer dermis. Inset: Merkel cell complexes (SA-I mechanoreceptors) are located at the tips of epidermal ridges. (**E**) Diagram of the TacTip with stiff artificial epidermis outer layer over a softer artificial dermis (clear silicone gel). Natural epidermal ridges are replicated with stiff pins protruding into the silicone gel. Inset: white markers from which artificial SA-I and RA-I afferents are derived, are fused to the pin tips.

quantities of local skin tissue to which natural and artificial afferents respond, and the factors contributing to spatial resolution in population coding. In addition to gaining insight into the capacity of artificial type-I afferents to mediate salient population codes, a novel methodology is introduced for psychophysical testing of robot touch using a well-established technique from psychology known as signal detection theory (SDT) [24] (Material and Methods).

2 Results

2.1 Experiment 1a: Response to Normal Pressure

This experiment was designed to understand the degree to which artificial SA-I and RA-I afferents model their natural counterparts when stimulated with a simple normal force applied by a flat surface. First, we consider adaption rates and compare the response of artificial type-I afferents to the firing rates of individual natural type-I afferents in several studies that use the same stimulation conditions [25, 26, 27, 28]. Following this comparison, we consider the spatial modulation of artificial afferent responses across the entire population. We asses the nature of the skin dynamics to which individual artificial afferents respond and make a preliminary hypothesis about the ability for these artificial

tactile channels to mediate population codes.

2.1.1 Artificial Type-I Afferents Model Natural Afferent Adaption Rates

Artificial SA-I afferents responded to the stimulus onset and hold phase but not the offset (Figures 3A,F). Artificial RA-I afferents responded strongly to the stimulus onset and offset but not the hold phase (Figures 3B,G). These patterns of activity are strongly indicative of their natural counterparts, which we now examine in more detail.

Natural SA-I afferent firing rates are known to increase with indentation depth [27]. This correlation between indentation depth and firing rate is mirrored in the artificial SA-I afferents, which demonstrate a trapezoid response curve with steady activity over the hold phase increasing with indentation depth (Figures 3A,F; both slow and fast presses). Further supporting the likeness of artificial SA-I afferents to their natural counterparts, both natural and artificial SA-I afferent responses fell to zero with removal of the stimulus [26, 27].

Natural SA-I afferents are known to fire maximally during the dynamic phase of the stimulus presentation, with a slow reduction of activity under constant stimulation (slow adaption) [26]. The artificial SA-I afferents diverged from this: artificial SA-I response rose steadily as the TacTip was pressed onto the stimulus, then sustained their maximal activity (*i.e.* had no slow adaption). We comment that all biological sensory systems adapt to stimulation for complex neurophysiological reasons (signalling pathways *etc*), whereas artificial sensors are designed for repeatable operation. It is reasonable that 'slow adaptation' becomes 'no adaptation'.

Natural RA-I afferents are known to respond only during dynamic phases of stimulus presentation, *i.e.* rapidly adapt during stimulus onset and offset [26]. In agreement with this pattern of adaptation, artificial RA-I afferents exhibited distinct transience: for both slow and fast presses, artificial RA-I channels responded only during the dynamic phases of the experiment (Figures 3B,G; slow and fast presses). Furthermore, the peak response of the artificial RA-I afferents was greater for fast presses. This behaviour is also indicative of natural RA-I afferents, which show monotonically increasing firing rates with increased indentation speed [28].

2.1.2 Individual Artificial Type-I Afferents Encode Local Shear and Population Response Encodes Shape

Both the artificial SA-I and RA-I afferents are good candidates for providing viable codes to represent static extended stimuli via spatial modulation, because the spatial arrangement of artificial responses provides information about the contact shape. This capability is also posited for the firing rates of both natural SA-I and RA-I afferents [20, 18].

The spatial arrangement of the artificial SA-I population response shows an approximately circular central region where minimal activity occurs, even at times of peak stimulation (Figures 3C,H; slow and fast presses). Radiating away from this central region, afferents exhibit increased activity. This spatial pattern can be understood by considering a basic physical model of the interaction between the biomimetic fingertip's skin and the stimulus: when the slightly-rounded tip is pressed onto a flat surface, a circular area of the tip compresses and conforms to the surface (Figures 4A,B; non-contact and stimulated tips). The size of this area depends on how strongly the fingertip is pressed onto the surface, with the markers away from the center spreading outwards as the skin flattens. Thus, the central SA-I afferent has minimal activity, which increases for afferents further way from the centre (Figures 4A,B; marker displacements increase radially).

At peak amplitudes of the artificial RA-I response, *i.e.* during the dynamic phase, the activity is also low in the central region and increases outwards (Figures 3D,I; 2nd and 4th images), giving an approximately radial population response. According to our model (Figures 4A,B), each marker moves in one direction during the press phase (towards the circumference) and in the opposite direction during the release phase (towards the centre). The artificial RA-I afferent response is a measure of

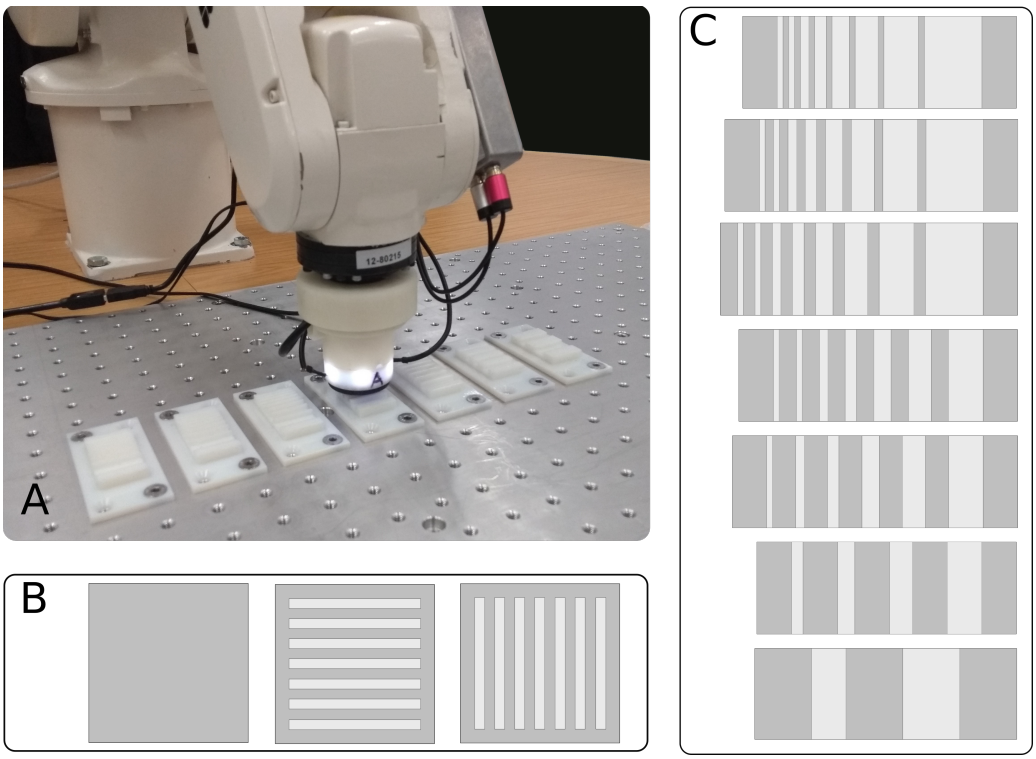

Figure 2: (**A**) Robot setup: TacTip mounted as an end-effector to the ABB robot arm, collecting data on aperiodic grating stimuli (Experiment 1b). (**B**) Plan view of flat plate stimulus (Experiment 1a and Experiment 2) (left); plan views of a periodic grating stimulus (Experiment 2) at two orthogonal orientations. (**C**) Plan view of the seven aperiodic gratings (Experiment 1b).

marker displacement per frame, which is the local shear-velocity magnitude. Thus, in this particular example, the spatial arrangements of artificial SA-I and RA-I responses are similar.

Given that our model of the biomimetic fingertip's skin (Figure 4) implies that individual artificial SA-I and RA-I afferents encode local shear strain, the spatial modulation of each artificial afferent response will depend on the local stimulation. Hence, the shape of the stimulus will determine the pattern of activity across the entire tip.

2.2 Experiment 1b: Response to Bars, Edges and Gratings

This experiment mirrors a classic (1981) neurphysiological study into peripheral neural representations of spatially complex tactile stimuli (edges and bars) in monkey primary afferents by Phillips and Johnson [16]. Preceded by a psychophysics study into human perception of tactile stimuli (including gratings) via spatial neural mechanisms [15], the purpose of their two studies was to understand the "coding mechanisms underlying the human's ability to resolve gratings".

Here we compare the activity of centrally-located artificial type-I afferents and natural type-I afferents taken from [16] when undergoing the same complex stimulation with grating stimuli (Table S1). In addition to comparing artificial and natural mechanoreception, we use this experiment in accordance with the original study to understand the biomimetic fingertip's ability to spatially resolve grating stimuli.

As in [16], results are displayed in the form of spatial-response profiles (SRPs). In the case of the measured artificial afferents, SRPs show the mean response over the entire pressing phase at each position, separated by 400 μm. We present the results in the context of three stimulus features, approximately mirroring the original study: *(i)* sensitivity to edges; *(ii)* sensitivity to bars; and *(ii)* the effect of neighbouring edges and bars.

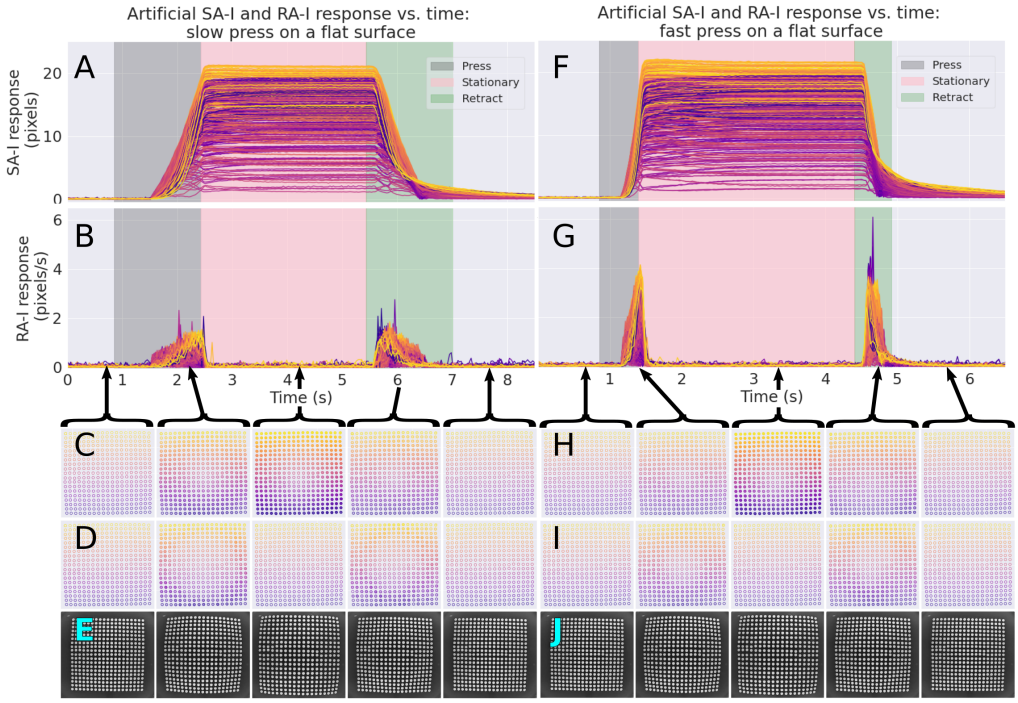

Figure 3: Artificial SA-I, RA-I response and image data collected during a press on a flat surface at slow 3 mms^{-1} (panels **A**-**E**) and fast 10 mms^{-1} motion speeds (panels **F**-**J**). (**A**,**F**;**B**,**G**) show the SA-I and RA-I responses vs time for slow and fast presses respectively. (**C**,**H**;**D**,**I**) show the spatial arrangement of SA-I afferents and RA-I afferents with their respective response profiles (depicted by opacity of each colour) at the indicated times. (**E**,**J**) show raw images of marker displacements at the same time instances as above.

2.2.1 Sensitivity to Edges

The central artificial SA-I afferent exhibits preferential sensitivity to "edges facing a large gap" (Figure 5A), which is a characteristic mirrored in natural SA-I afferents [16]. This pattern is most clearly seen in panel A7, where the response of natural and artificial SA-I afferents were attenuated by three bars and amplified by the six associated edges. This characteristic is also seen on the approach and departure for each of the other gratings, where the gratings exhibit rising and falling edges before and after free space respectively.

Likewise, the central artificial RA-I afferent exhibits preferentially sensitivity for edges (Figure 5B). (Note that SRPs are not shown for natural RA-I afferents because they were only available in [16] for some stimuli.) This distinguishes the measured artificial RA-I afferent from its natural counterpart, which was not observed to show any evidence of edge enhancement [16]. That said, the degree of edge enhancement for the artificial RA-I afferents was lower than that of artificial SA-I afferents and modulated around an overall high-level of activity, which is most noticeable on stimuli 6 and 7 (panels B6,7).

In the case of artificial afferents, edge enhancement can be explained with our basic model of local shear strain within the biomimetic fingertip (Figure 4). For an edge stimulus, the marker undergoes shear strain due to levering of the papillae-like nodule as the skin bends, causing both the artificial SA-I and RA-I afferents to respond (Figures 4C,D).

Phillips and Johnson hypothesised that the difference in SRPs between natural SA-I and RA-I afferents was a consequence of an "intrinsic difference in the spatial organization of their receptor mechanisms" [16]. However, in our study the spatial arrangement of receptive fields of artificial SA-I and RA-I afferents are necessarily identical, being derived from the same markers. Why then do the artificial RA-I afferents still respond less strongly? Instead, we attribute this to small perturbations in

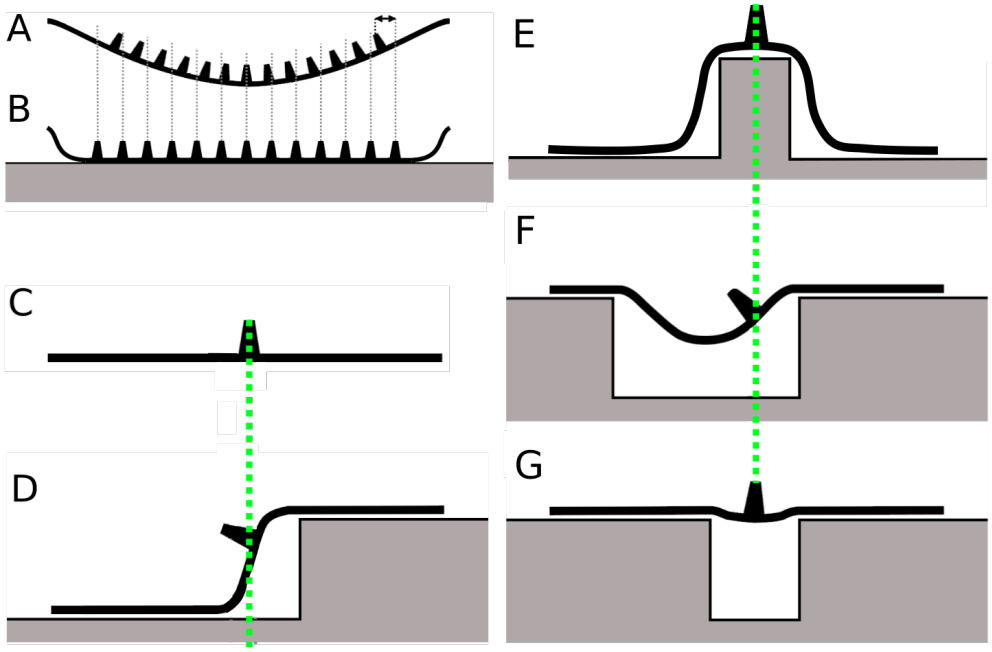

Figure 4: (**A**,**B**) Simplified diagram of TacTip deformation when pressed onto a flat plate. (**A**) At rest, *i.e.* no deformation, and (**B**) pressed flat. (**C**-**G**) Simplified diagram of the TacTip's central artificial afferent pressed onto features of aperiodic gratings: at rest (**C**), an edge (**D**), an isolated bar (**E**), and an edge neighbouring two gaps (**F**,**G**).

marker position which happen very quickly during the initial and final stages of the press. (For example, from low amplitude transient pressure waves in the sensor or inaccuracies in the setup causing micro shear forces even on a flat surface.) Due to their low amplitude and short time-scale, when taking the derivative, these perturbations will be amplified with respect to the more sustained response, *i.e.* the shear strain from an edge stimulus. Thus, the artificial RA-I responses shows less edge enhancement due to a higher *noise floor*. If, like artificial afferents, natural SA-I and RA-I afferents are responsive to some specific skin dynamic and its rate of change respectively, as suggested in [29], it is possible that reduced edge enhancement in natural RA-I afferents is also simply a consequence of noise amplification.

2.2.2 Sensitivity to Bars

A consequence of amplified edge response, seen in both natural SA-I and artificial SA-I and RA-I afferents, is a comparatively diminished response to isolated bars. Diminished response to isolated bars is limited to broad bars only for natural SA-I afferents, where single peaks are observed due to some narrow isolated bars (Figure 5, panel A1, A2); however, the central artificial SA-I afferent appears to respond exclusively to edges.

The exclusive response of artificial type-I afferents to edges can again be understood with a shear model of TacTip skin dynamics (Fig 4). Bars can be considered flat surfaces and thus, when the artificial afferent is located directly above the bar it will not produce any response in said afferent, regardless of bar width (Figure 4E). (However, in practice some response is still observed, in particular in artificial RA-I afferents, which we attribute to transient contact induced pressure or inaccuracies in the experimental setup.)

This is an intriguing result which alludes to some differences in either the precise skin dynamics to which natural and artificial type-I afferents respond or additional population processing in the periphery of the natural somatosensory system prior to recording. Nevertheless, for the purpose of understanding neurophysiology of touch, it highlights the value in comparing the response of individual artificial afferents in a biomimetic tactile sensor to their natural counterparts.

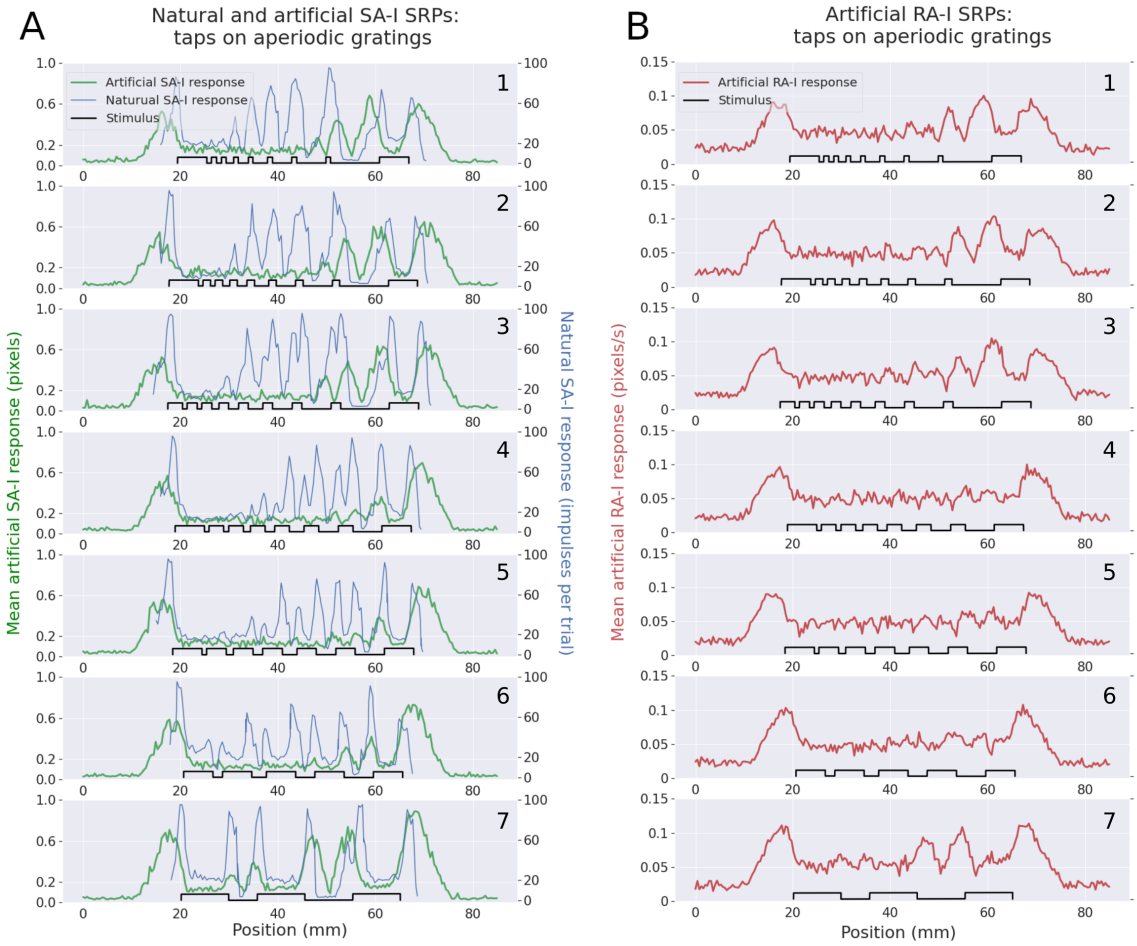

Figure 5: (**A**) Stimulus response profiles for a single monkey SA-I afferent collected on seven gratings taken from Phillips and Johnson [16] and corresponding SRPs for the central artificial SA-I afferent (green) collected on gratings (black). (**B**) SRPs for the central RA-I afferent (red) collected on gratings (black). In A and B, grating dimensions used with artificial afferents (x-axis) are doubled compared with those used with natural afferents in [16].

2.2.3 Effect of Neighbouring Bars and Edges

The sensitivity of both individual natural and artificial type-I afferents to edge and bar features was attenuated with reduced gap width. For example, both natural and artificial SA-I afferents show reduced edge amplification from right to left as gaps between the edges become smaller (Figure 5A).

For artificial afferents, this attenuation can be explained by extending our basic model of the biomimetic fingertip (Figure 4). The amount of marker deflection is reduced with decreasing gap width owing to a finite flexibility of the fingertip's skin. In essence, the skin acts as a low-pass filter that attenuates the response to high spatial frequencies of the stimulus (Figures 4E,F,G; central marker on an edge with reducing gap width).

In the original experiments, it was observed that "as the bars are spaced more closely than 3.0 mm the heights of the associated response peaks are diminished" [16]. Likewise, the artificial SA-I afferents show diminished response peaks for narrower gap widths (Figure 5A). This effect is more pronounced for the artificial afferents than their natural counterparts because of a larger length scale where artificial edge responses begin to be diminished (visible at 10 mm in aperiodic gratings 1, 2, 3 and 7, and 6 mm in aperiodic gratings 4, 5 and 6). In all cases, the associated peaks become increasingly diminished as gaps become smaller until SRPs do not represent spatial structure of the stimulus; instead, the natural and artificial SA-I afferents respond as though the stimulus were an individual bar or flat surface. This effect occurred at gap widths of $\lesssim$1 mm and $\lesssim$3 mm for natural and artificial SA-I afferents respectively.

Both natural and artificial RA-I afferents also exhibit attenuation in the amount of stimulus detail represented within their associated SRPs with reducing gap width (Figure 5B for artificial RA-I afferent SRPs; see [16] for natural RA-I afferent SRPs). Furthermore, both natural and artificial RA-I afferents exhibit faster attenuation in response to reducing gap width than their SA-I counterparts. For natural RA-I afferents, "the profiles of all five fibers were clearly modulated by the 5.0 mm gap in the stimulus, but gaps of 0.5-1.0 mm were not represented in any of the five profiles" [16]. The central artificial RA-I afferent profile similarly shows modulation to 10 and 6 mm gaps but edges bounded by gaps of 1-4 mm were not represented.

Therefore, the effect of neighbouring edges and bars appears to be similar for natural and artificial type-I afferents, except the length scale for artificial afferents is larger (6-10 mm) than for natural afferents (3.0 mm). We attribute this to differing dynamic properties of natural and artificial skin: the artificial skin is thicker and less flexible than its natural counterpart. Other than this difference, there was significant convergence between the artifical and natural systems.

2.3 Experiment 2: Grating Resolution

This experiment mirrors a classic (1981) two-interval same-different psychophysical task carried out by Johnson and Phillips [15], where the ability for human participants to discriminate grating orientation is affected by spatial periods of the grating stimuli. We use an identical set of seven periodic grating stimuli with grating periods ranging from 1 to 5 mm and we use an additional eighth stimulus with a grating period of 0 mm (completely flat), essentially as a control (Figure 6; left column). Grating orientation was of particular interest because non-spatial stimulus features, *e.g.* total stimulus area and edge content, are consistent between the first and second interval of each trial ($\psi = \pm 45°$), thus inhibiting non-spatial mechanisms [15]. For this reason, many experimenters have subsequently used grating orientation as a tool for measuring tactile spatial acuity [30, 31, 32].

First, we consider the structure of artificial SA-I and RA-I tactile images when stimulated with gratings, in relation to their ability to spatially-resolve grating stimuli. Following, we examine the psychometric functions for artificial SA-I and artificial RA-I afferents resulting from performing the two-interval same-different grating resolution task with the robot in terms of their ability to spatially resolve grating stimuli in comparison with human performance.

2.3.1 Artificial SA-I Spatial Structure Increases with Grating Period

The efficacy of the artificial SA-I afferent population for transducing grating orientation through spatial structure was attenuated by a reduction in grating period: artificial SA-I images have a visible fine-spatial structure only for the coarser gratings with periods of 3 mm or more (Figure 6, centre column). SA-I tactile images from periods of 2.5 mm or less exhibit a diminished structure, appearing qualitatively similar in having a central dark region of relatively low response within an active surround (aside from unimportant variations in the location of the central region, due to the experimental protocol of perturbing randomly the contact location and angle). In particular, SA-I tactile images collected on gratings with periods 0-2.5 mm do not appear to show any structure that indicates the grating orientation.

This attenuation in spatial structure of artificial SA-I tactile images appears, in-part, to be a consequence of the same effect that produced spatial attenuation in Experiment 1b (response to bars, edges and gratings). For the artificial afferents, we explained this effect with a basic model of the biomimetic fingertip, in which the tangential stiffness of the skin means it cannot perfectly conform to narrow ridges (Figure 4). Qualitatively, the same effect appears here.

There is, however, a curious mismatch between the spatial sensitivity of the tactile images in this Experiment 2 and that of a single SA-I artificial afferent in Experiment 1b. Spatial frequencies of 2.5 mm or more are perceivable for gratings with gap widths of 1.25 mm or more (Figure 6, centre

column); however, spatial features were not distinguishable at 3 mm or less on the ridged stimuli (Figure 5, centre row). It seems that the nature of the spatial filtering applied by the skin has a complex relation to the relative geometry between local skin and the stimulus features. The primary feature of all artificial SA-I tactile images stimulated by a flat stimulus was low response in the centre of each image with increasing response radiating away from this central region (Experiment 1a) as predicted from the SRPs (Figure 5). However, in gratings with spatial frequencies of 2.5 mm or more, the majority of grating-like structure is seen on the periphery of the tactile images where the afferent response is usually greater. More specifically, the most salient regions of tactile images are the top right and bottom left for $\psi = -45°$ and vice versa for $\psi = 45°$. Thus, the skin is more able to conform to aspects of the local stimulus structure where the grating orientation is orthogonal to direction of greatest slope of the TacTip's resting skin shape (corresponding to the radial direction; see Figure 4A).

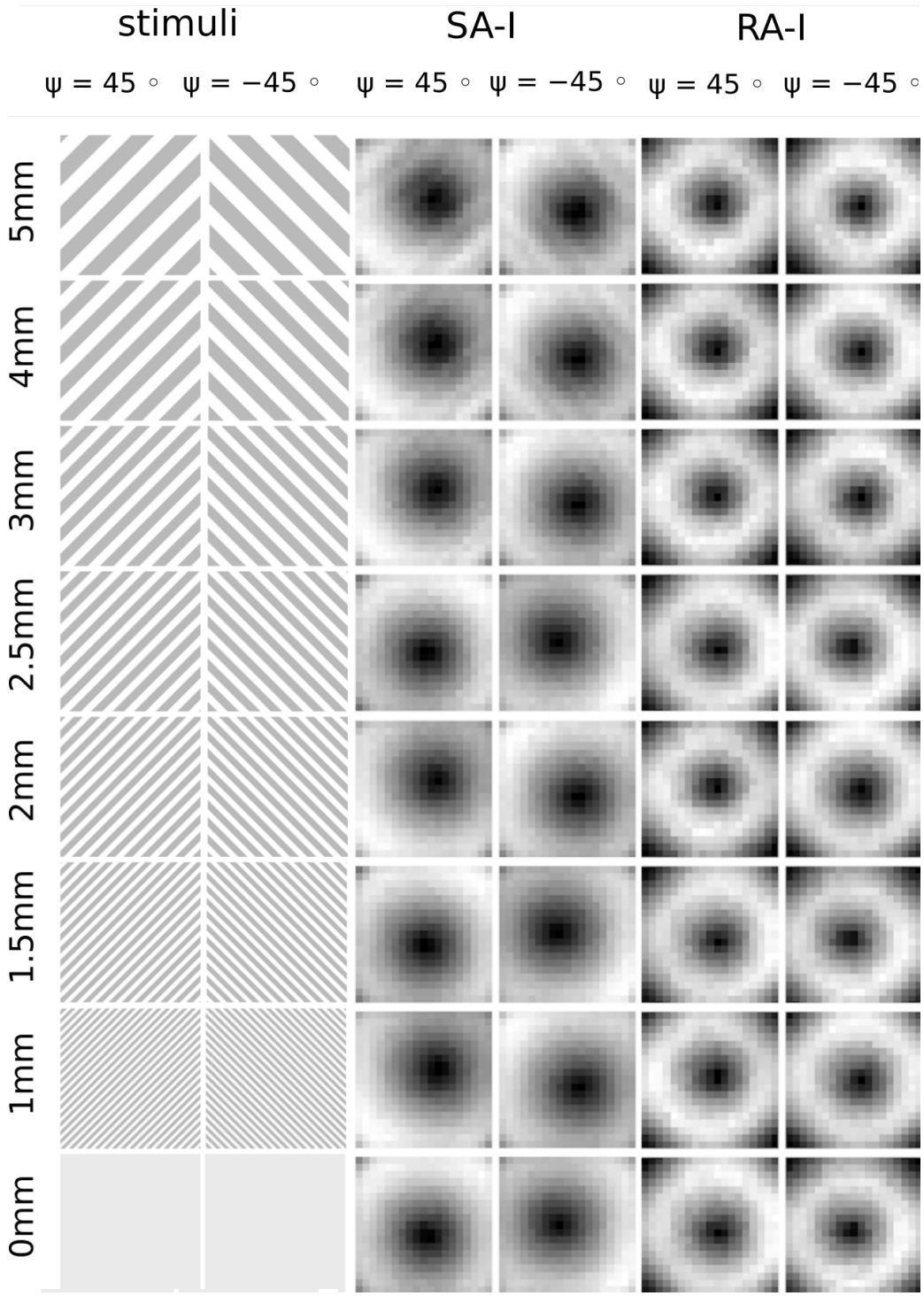

Figure 6: Examples of artificial SA-I and RA-I tactile images (centre and bottoms rows) collected on grating stimuli (to same scale; top rows). For each grating period (0-5 mm), both possible orientations ($-45°$ and $45°$) are displayed. The colour of each pixel represents the response of the associated artificial afferent: lighter corresponds to higher responses.

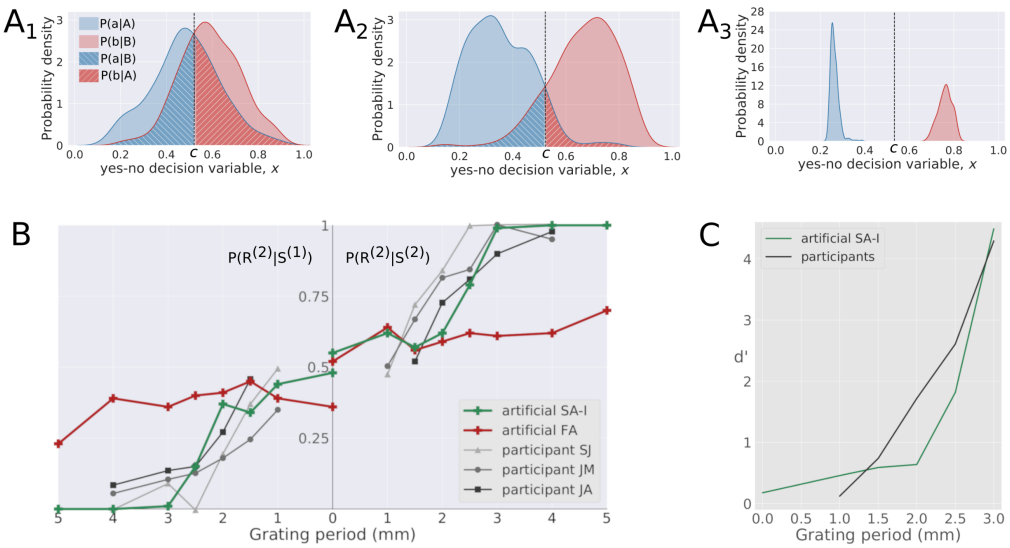

Figure 7: (**A**$_1$,**A**$_2$,**A**$_3$) Yes-no SDT covert decision models for artificial SA-I afferents in the grating orientation two-interval same-different task, with grating periods of 0, 2.5 and 5 mm respectively. (**B**) Robot (artificial SA-I and RA-I) and human psychometric functions for grating resolution, two-interval same-different task, according to the conditional probabilities for responding 'different' ($R^{(2)}$) given a different stimulus presentation in the second interval ($S^{(2)}$; right) or given the same stimulus presentation ($S^{(1)}$; left). (**C**) Behavioral separation index (d') versus grating period for the decision model according to artificial SA-I afferents compared with mean of human participants.

2.3.2 Artificial RA-I Images do not Resemble Grating Orientation

Unlike artificial SA-I images, the RA-I images do not exhibit any visible spatial structure indicative of orientation of grating stimuli (Figure 6, right). All artificial RA-I tactile images appear indistinguishable (aside from unimportant variations in the location and size of the central dark region, for the same reasons as for the SA-I afferents).

At first sight, this lack of grating-like structure in artificial RA-I tactile images would seem related to the relative lack of detail exhibited in single artificial RA-I afferent activity in Experiment 1b (Figure 5B) compared to artificial SA-I activity (Figure 5A). While this effect may have contributed, it is also likely that the data preparation also contributed. Tactile images were constructed from the single frame which produced the highest total response for each press (Methods). For artificial RA-I afferents this is likely to be somewhere near the middle of the press whereas for SA-I this is likely to be at the bottom of a press. It appears that the TacTip skin begins to conform to the grating structure at later stages of the press when pressure is greater.

2.3.3 Artificial SA-I Afferents Outperform Artificial RA-I Afferents in Grating Resolution Task

Mirroring the original study [15], we implemented a *robot psychophysical* two-interval same-different task, where our artificial tactile system was "required to judge whether two gratings with the same period, presented sequentially, were presented with the same alignment, $S^{(1)}$, or with orthogonal alignments, $S^{(2)}$" [15]. More explicitly, $S^{(1)}$ and $S^{(2)}$ correspond to AA and AB respectively where A corresponds to $\psi = -45°$ and B corresponds to $\psi = 45°$ (see Figure 6).

We implemented two artificial decoders from convolution neural networks for artificial SA-I and RA-I afferents which were proposed to decode grating angle encoded spatially within tactile images of artificial SA-I and RA-I response. Decision making was performed by using methods from SDT and equating the continuous output of these artificial decoders to a *decision variable* (Methods).

In psychophysics, the *just-noticable difference* (JND), also called the distance threshold, is a standard metric of perceptual performance that corresponds to measuring the amount a stimulus must change for the difference to be noticeable. Here, it is defined as the grating period at which humans and the robot gave a correct response 75% of the time in the task. JNDs are ∼2.4 mm and >5 mm for artificial SA-I and artificial RA-I afferents respectively (Figure 7B).

Conditional probabilities of responses, $P(R^{(2)}|S^{(2)})$ and $P(R^{(2)}|S^{(1)})$, for artificial SA-I afferents approximate a sigmoid function, typical of psychometric data. 100% of responses were correct for grating periods $\lesssim$3 mm (Figure 7B). In contrast, the psychometric function for artificial RA-I afferents does not demonstrate any clear improvement above baseline level within the scale of grating period used in this experiment (Figure 7B). This result is in agreement with the observation from artificial RA-I tactile images that they do not reflect grating orientation (Figure 6). It seems plausible that tactile images constructed from artificial RA-I afferent response contain little to no spatial information that encodes grating orientation.

The finding that artificial SA-Is outperform artificial RA-Is is consistent with human touch: Johnson and Phillips observed that by vibrating stimuli at 40 Hz, in order to additionally excite RA-I afferents, there was only a very small improvement in the performance of participants in the grating orientation task [15].

2.3.4 Artificial SA-I Performance is Comparable with Humans

Artificial SA-I attained perfect performance where grating periods were $\geq$3 mm, which is roughly comparable with performance of the three human participants who reached near perfect performance at grating periods of 2.5-4 mm, depending on the participant (Figure 7B). Comparable JNDs were observed: JNDs for participants SJ, JM and JA were ∼1.7, 1.7 and 2.1 mm respectively, compared with ∼2.4 mm for artificial SA-I afferents (Figure 7B).

Johnson and Phillips stress the relevance of the presented grating resolution task due to the full range of performance (0.5-1) between chance and perfect discrimination. Chance-level was attained at grating periods of 1 mm, leading the authors to conclude that purely spatial mechanisms are responsible for the decision performance in the human grating resolution task [15]. Although the full range of performance was not quite observed for artificial SA-I afferents (Figure 7B, range 0.55-1), the sensitivity index (a dimensionless statistic indicating the discriminability of $S^{(1)}$ and $S^{(2)}$; for its calculation see SI appendix), d', for artificial SA-I afferents demonstrates a similar relationship to grating period as that of humans, where grating periods are $\geq$2 mm (Figure 7C). Above-baseline performance on the smooth stimulus is likely to be caused by some *non-grating cue* which systematically varies with the sensor's angle relative to the stimulus and is available on all stimuli. The relationship between d' and grating period for artificial SA-I afferents demonstrates this *dual-cue* mechanism (Figure 7C) where d' is relatively consistent for grating periods $\leq$2 mm ($\sigma_{d'}$ = 0.24), an inflection point is observed at grating periods of 2 mm, above which the d′ gradient increases significantly owing to the availability of the more salient population code of grating cues ($\sigma_{d'}$ = 1.97). Above the critical grating period (2 mm), the primary feature driving perception is a population code of grating orientation and thus it seems plausible that similar spatial mechanisms are responsible for the decision process in humans and the robot.

3 Discussion

In human touch, the importance of mechanical variability of the transformation of stimuli into the response of primary afferents located in the skin has been acknowledged [33], although the precise aspects of contact-induced skin dynamics to which primary afferents respond is not yet fully understood. Likewise, for artificial touch, the responses of individual afferents greatly affected the tactile images and thus the ability to reliably decode stimulus properties. We demonstrated that the shear

strain model of the TacTip (Figure 4) accounts for much of the similarity between artificial and natural type-I afferent SRPs, in particular the preferential sensitivity of SA-I afferents for edges, the attenuation in response with reducing gap width, and the reduced sensitivity of RA-I afferents (Experiment 1b: Response to bars, edges and gratings).

Natural SA-I afferents, however, were responsive to narrow bars whereas artificial SA-I afferents were responsive exclusively to edges. One explanation for this discrepancy is a different aspect of skin dynamics to which natural and artificial afferents respond at the length scale of narrow bars. Indeed, a subsequent study by Phillips and Johnson (1981) [34] found that natural SA-I and RA-I afferent SRPs were most closely correlated with continuum mechanics models of compressive and tensile strain respectively. That said, the true nature of contact mechanics at the length scales of mechanoreceptors may differ from those of the macroscopic laws of continuum mechanics due to assumptions in the models [6]; for example, inhomogeneities in skin structure may be important at the scale of mechanoreceptors [35].

The spatial sensitivity to gratings is similar to the artificial afferent spacing (1.2 mm), as spatial frequencies of 2.5 mm are clearly distinguishable in Experiment 2 corresponding to gap widths of 1.25 mm. Although the perception of grating orientation is poorer for finer gratings, there is some improvement in the range 0-2 mm, which we attribute to hyperacuity due to spatial mechanisms arising from population coding. Tactile hyperacuity has been observed in other studies of artificial touch, where it is considered a biomimetic form of superresolution [36, 37]. It is tempting to invoke a lack of physical resolution as an explanation for why single SA-I afferent SRPs in Experiment 1b could not distinguish spatial features at 3 mm on the ridged stimuli (compared with 1.25 mm gap widths for gratings). However, we do not view population coding as the sole difference in this case, as there also seems to be subtle spatial filtering affects depending on the relative geometry between skin and local stimulus features that affect the ability to conform to local stimulus structure.

Regardless of important details such as the nature of mechanoreceptor responses, the coding schemes within individual afferents, and the neural processing involved in population coding, the present study has demonstrated the value in examining population codes of biomimetic artificial tactile sensors and a careful comparison to the natural systems which they aim to mimic. As the fields of neuroscience and robotics continue to converge, there is an opportunity to improve artificial tactile perception and build knowledge of natural touch with potentially important future implications for robotic manipulation, neuroprosthetics and the neurophysiology of touch.

4 Methods

4.1 Sensor Design

Here we describe the key operating principles of the TacTip biomimetic optical tactile sensor. For the manufacturing procedure please refer to SI appendix. For a detailed explanation of the design concepts, we refer the reader to a paper on 'the TacTip family' by Ward-Cherrier et al. (2018) [9].

The TacTip (Figure 1C) features a black flexible skin covering a clear silicone gel (Figure 1E). The artificial epidermis and dermis provide contrasting stiffness which is proposed to mimic the corresponding layers of natural skin. The artificial epidermis is initially completely flat although, once the tip is filled with gel, forms a slight convex bulge owing to pressure within the tip (Figure 4A; cross-sectional diagram of unstimulated tip).

In the human fingertip, Merkel cell complexes (SA-I afferents) are situated in the dermis at the tips of stiff epidermal ridges which protrude into the softer dermis (Figure 1D). This morphology is mimicked in the TacTip with stiff epidermal pins that protrude into the soft gel. A white marker on the tip of each pin provides an optical signature of local shear strain imaged using a USB camera (Figure 1C) (Figure 4); although the use of optics is clearly non-biomimetic, we consider the skin morphology and transduction of contact to be based on the physiology of human skin. 361 white markers arranged

in a 19×19 square grid ($\sim$500 mm^2) yield a marker density of $\sim$70 cm^{-2} ($\sim$1.2 mm separation) which is approximately half the innervation density of type-I afferents in the human fingertip [22, 23].

4.2 Feature Extraction

4.2.1 Artificial SA-I Afferents

Firing rates of natural SA-I afferents are modelled using marker displacements (shear-strain magnitude), since these should remain consistent with sustained deformation, thus modelling slow adaption.

4.2.2 Artificial RA-I Afferents

To account for the phasic nature of Meisner corpuscles, RA-I firing is modelled as marker speed. This model is similar to other proposed transduction models of RA-I firing, where the first derivative of pressure is used as the primary input to a biological neuron model [38, 39, 40].

4.3 Experiment 1a: Response to Normal Pressure

4.3.1 Collection Procedure

The same robotic platform is used for all experiments. Details are provided in SI appendix. The TacTip begins in free-space at 2 mm above a flat 3D-printed surface (Figure 2B left). Video data is recorded from the TacTip as the TacTip is simultaneously moved downward until a compression of 2.5 mm is achieved. At the bottom of the press the TacTip is held stationary for 3 seconds before returning to its initial position where recording is terminated. To examine the effects of stimulation speed on artificial afferent response, the data collection procedure is repeated twice with the robot moving at 3 and 10 mms^{-1}. Artificial SA-I and RA-I responses are extracted off-line for each frame subsequent to data collection as described in *Feature Extraction* above.

4.4 Experiment 1b: Response to Bars, Edges and Gratings

4.4.1 Stimuli

A set of seven 3D-printed gratings (Figure 2C and SI appendix, Table S1) corresponding to those in the experimental study [16] are used. Bar and gap widths vary in the same proportions as those used in [16]; however the scaling is doubled, thus all bars and gaps are twice as wide. This scaling was chosen because the innervation density of markers in the TacTip ($\sim$70 cm^{-2}) is approximately half that of SA-I afferents in the human fingertip.

4.4.2 Collection Procedure

The TacTip is successively pressed onto a stimulus indenting the skin by 1 mm, with each press taking $\sim$0.8 s. The TacTip is held stationary at the bottom of a press for 0.5 s. Between each press the TacTip is moved 200 μm perpendicular to the bar/gap axis, starting in free space on the left-hand side of the stimlus and moving over the entire stimulus until free space is again reached. Tactile image data is recorded for the entire downward phase and stationary period of each press. This process is repeated seven times, once for each stimulus. Artificial SA-I and RA-I responses are extracted off-line as described in *Feature Extraction* above.

4.5 Experiment 2: Grating Resolution

4.5.1 Stimuli

Seven square-wave grating stimuli were produced by cutting grooves (depth 1.5 mm) in plastic blocks with a CNC milling machine (example depicted in Figure 2B). The periodicity of the gratings, 1, 1.5, 2, 2.5, 3, 4 and 5 mm, correspond to those used in the analogous psychophysical grating resolution experiment [15]. Additionally, we use an eighty completely smooth surface, considered as a grating of periodicity 0 mm.

4.5.2 Collection Procedure

Data are collected by pressing the TacTip skin onto the grating stimuli so that a compression of 2.5 mm is achieved, after which it is held stationary for 1 s. Tactile image data is recorded for the entire downward phase and stationary period of the press.

For each grating, data is collected in two distinct phases: one for training and validation, the other for testing. For training and validation, the yaw angle, ψ, of the sensor relative to each grating is treated as a label, and randomly sampled from a uniform distribution within a 180°range, $-90° \leq \psi \leq 90°$, by rotating the wrist joint of the robot. The extremes $\psi = \pm 90°$ are arranged so that grating grooves align with the rows/columns of TacTip markers.

Roll (ϕ), pitch (θ), x, y and z are randomly sampled within ranges $\pm 2°$, $\pm 2°$, ± 2.5 mm, ± 2.5 mm and ± 0.15 mm respectively, but not retained as labels for the data. We introduce this variability to avoid systematic variation in these dimensions as a consequence of variation in the rotation angle ψ, which the neural network could otherwise use to distinguish grating orientation.

The training/validation set consists of 1000 samples per grating, giving a total of $N = 7000$ samples.

Seven distinct test sets are collected, one for each grating. On each grating, 300 samples are collected at $\psi = -45°$ and 300 samples are collected at $\psi = 45°$. We denote these, conditions A and B, such that stimuli A and B are perpendicular and equidistant from the lower (-90°) and upper (90°) bounds of the training data. As with the training data, ϕ, θ, x, y and z are all randomly sampled within their above ranges.

4.5.3 Sample Preparation

For training, validation and testing, artificial SA-I and RA-I responses are extracted off-line for each frame as described in *Feature Extraction* above.

SA-I and RA-I samples are tactile images of their respective afferent responses over the surface of the tip (Figure 6). In both cases, for each press, only the frame with largest total response across the tip is used for the analysis.

4.5.4 Perceptual Model and Training

For predicting the angle ψ, two convolutional neural network (CNN) regression models, CNN-SA1 and CNN-RA1, for artificial SA-I and artificial RA-I afferents respectively are implemented. CNN-SA1 and CNN-RA1 are trained to predict ψ using their respective afferent responses extracted from training data on all seven gratings ($N_{\text{train}} = 5250$) and likewise validated on all seven gratings ($N_{\text{val}} = 1750$). Details of model architecture and training procedure are provided in SI appendix.

4.5.5 Testing: SDT Model of Two Interval Same-Different Task

Here we describe the general approach of how signal detection theory (SDT) may be used with robotics and in particular how this applies to the *two-interval same-different* grating resolution task.

A formal description of the exact method used in this study is provided in the SI appendix.

The *two-interval same-different* task is a psychophysical paradigm where participants are presented with two intervals per trial, with each interval presenting either stimulus A or stimulus B. Participants are required to respond by stating whether the stimuli in the two intervals were the same or different [41].

In the robot psychophysical task, A and B are $\psi = -45°$ and $45°$ respectively. Mirroring a psychophysical grating resolution experiment (Johnson and Phillips (1981) [15]), the possible presentations on each trial are either AA or AB, which we refer to as $S^{(1)}$ and $S^{(2)}$ respectively.

SDT is used to relate perception to sensitivity of sensory-driven neural activity. Central to SDT is the *decision variable*, which is an interpretation of neural activity that guides decision making [42]. The process of forming a decision variable from neural activity is often referred to as decoding (Figures 1A, 1B; decoding phase). In SDT, the decision variable is compared to a criterion value for decision making. Our approach to robot decision making for the two-interval same-different task is underpinned by equating the continuous output of regression models to the decision variable of SDT.

First, probability distributions, $f(x \mid \mathrm{A})$ and $f(x \mid \mathrm{B})$ (Figure $7A_{1\text{-}3}$), are constructed from the output of the trained SA-I regression model when presented with all 300 test samples at $\psi = \pm 45°$ respectively. From these distributions, we follow a standard SDT framework for the two interval same-different task, characterised by individual *yes-no covert decisions* for each interval [43, 41], in order to attain the true positive ($P(R^{(2)}|S^{(2)})$) and false positive ($P(R^{(1)}|S^{(2)})$) rates for each grating period.

SDT deals with the problem of where to place the criterion value, c, representing the decision goals sought by the observer. For yes-no covert decisions, we use a simple decision goal to maximise the percentage of correct responses, *i.e.* to equally reward correct responses (a given A and b given B) and to equally penalise incorrect responses (a given B and b given A). The criterion value for this decision rule is shown in Figures $7A_{1\text{-}3}$.

Acknowledgements:
This research was funded by a Leverhulme Research Leadership Award on 'A biomimetic forebrain for robot touch' (RL-2016-39).

References

[1] Rolf Pfeifer, Max Lungarella, and Fumiya Iida. The challenges ahead for bio-inspired 'soft' robotics. *Communications of the ACM*, 55(11):76–87, November 2012. 330.

[2] Tony J. Prescott, Nathan Lepora, and Paul F. M. J. Verschure. *Living machines: A handbook of research in biomimetics and biohybrid systems*. Oxford University Press, April 2018.

[3] R.S. Dahiya, G. Metta, M. Valle, and G. Sandini. Tactile Sensing—From Humans to Humanoids. *IEEE Transactions on Robotics*, 26(1):1–20, February 2010. 1300.

[4] Chiara Lucarotti, Calogero Maria Oddo, Nicola Vitiello, and Maria Chiara Carrozza. Synthetic and Bio-Artificial Tactile Sensing: A Review. *Sensors*, 13(2):1435–1466, February 2013. 220.

[5] J. Scheibert, S. Leurent, A. Prevost, and G. Debrégeas. The Role of Fingerprints in the Coding of Tactile Information Probed with a Biomimetic Sensor. *Science*, 323(5920):1503–1506, March 2009. 200.

[6] Jonathan Platkiewicz, Hod Lipson, and Vincent Hayward. Haptic Edge Detection Through Shear. *Scientific Reports*, 6:23551, March 2016.

[7] B. P. Delhaye, E. W. Schluter, and S. J. Bensmaïa. Robo-psychophysics: Extracting behaviorally relevant features from the output of sensors on a prosthetic finger. *IEEE Transactions on Haptics*, 9(4):499–507, 2016.

[8] Z. Kappassov, J.-A. Corrales, and V. Perdereau. Tactile sensing in dexterous robot hands: a review. *Robotics and Autonomous Systems*, 74:195 – 220, 2015.

[9] Benjamin Ward-Cherrier, Nicholas Pestell, Luke Cramphorn, Benjamin Winstone, Maria Elena Giannaccini, Jonathan Rossiter, and Nathan F. Lepora. The TacTip Family: Soft Optical Tactile Sensors with 3D-Printed Biomimetic Morphologies. *Soft Robotics*, 5(2):216–227, April 2018.

[10] Clementine M. Boutry, Marc Negre, Mikael Jorda, Orestis Vardoulis, Alex Chortos, Oussama Khatib, and Zhenan Bao. A hierarchically patterned, bioinspired e-skin able to detect the direction of applied pressure for robotics. *Science Robotics*, 3(24), November 2018. 150.

[11] Calogero Maria Oddo, Stanisa Raspopovic, Fiorenzo Artoni, Alberto Mazzoni, Giacomo Spigler, Francesco Petrini, Federica Giambattistelli, Fabrizio Vecchio, Francesca Miraglia, Loredana Zollo, Giovanni Di Pino, Domenico Camboni, Maria Chiara Carrozza, Eugenio Guglielmelli, Paolo Maria Rossini, Ugo Faraguna, and Silvestro Micera. Intraneural stimulation elicits discrimination of textural features by artificial fingertip in intact and amputee humans. *eLife*, 5:e09148, March 2016. 200.

[12] J. A. George, D. T. Kluger, T. S. Davis, S. M. Wendelken, E. V. Okorokova, Q. He, C. C. Duncan, D. T. Hutchinson, Z. C. Thumser, D. T. Beckler, P. D. Marasco, S. J. Bensmaia, and G. A. Clark. Biomimetic sensory feedback through peripheral nerve stimulation improves dexterous use of a bionic hand. *Science Robotics*, 4(32), 2019.

[13] C. Chorley, C. Melhuish, T. Pipe, and J. Rossiter. Development of a tactile sensor based on biologically inspired edge encoding. In *2009 International Conference on Advanced Robotics*, pages 1–6, 2009.

[14] Romain Brette. Philosophy of the spike: Rate-based vs. spike-based theories of the brain. *Frontiers in Systems Neuroscience*, 9:151, 2015.

[15] K. O. Johnson and J. R. Phillips. Tactile spatial resolution. I. Two-point discrimination, gap detection, grating resolution, and letter recognition. *Journal of neurophysiology*, 46(6):1177–1192, 1981.

[16] J. R. Phillips and K. O. Johnson. Tactile spatial resolution. II. Neural representation of Bars, edges, and gratings in monkey primary afferents. *Journal of Neurophysiology*, 46(6):1192–1203, 1981.

[17] C E Connor, S S Hsiao, J R Phillips, and K O Johnson. Tactile roughness: neural codes that account for psychophysical magnitude estimates. *The Journal of neuroscience : the official journal of the Society for Neuroscience*, 10(12):3823–36, 1990.

[18] M. A. Srinivasan and R. H. LaMotte. Tactile discrimination of shape: responses of slowly and rapidly adapting mechanoreceptive afferents to a step indented into the monkey fingerpad. *Journal of Neuroscience*, 7(6):1682–1697, 1987.

[19] M. A. Srinivasan and R. H. LaMotte. Tactual discrimination of softness. *Journal of Neurophysiology*, 73(1):88–101, 1995.

[20] A. W. Goodwin, V. G. Macefield, and J. W. Bisley. Encoding of object curvature by tactile afferents from human fingers. *Journal of neurophysiology*, 78 6:2881–8, 1997.

[21] N. Cauna. Nature and functions of the papillary ridges of the digital skin. *The Anatomical record*, 119 4:449–68, 1954.

[22] Roland S. Johansson and Ake B. Vallbo. Tactile sensory coding in the glabrous skin of the human hand. *Trends in Neurosciences*, 6:27 – 32, 1983.

[23] R. Johansson and AB Vallbo. Tactile sensibility in the human hand: Relative and absolute density of four types of mechanoreceptive units in glabrous skin. *The Journal of physiology*, 286:283–300, 02 1979.

[24] D. M. Green and J. A. Swets. *Signal detection theory and psychophysics*. Wiley, New York, 1966.

[25] Hannes P. Saal, Benoit P. Delhaye, Brandon C. Rayhaun, and Sliman J. Bensmaia. Simulating tactile signals from the whole hand with millisecond precision. *Proceedings of the National Academy of Sciences*, 2017.

[26] Per Jenmalm, Ingvars Birznieks, Antony W. Goodwin, and Roland S. Johansson. Influence of object shape on responses of human tactile afferents under conditions characteristic of manipulation. *European Journal of Neuroscience*, 18(1):164–176, 2003.

[27] Vernon B. Mountcastle, William H. Talbot, and Hans H. Kornhuber. *The Neural Transformation of Mechanical Stimuli Delivered to the Monkey's Hand*, chapter 19, pages 325–351. John Wiley & Sons, Ltd, 1966.

[28] M. Knibestöl. Stimulus response functions of rapidly adapting mechanoreceptors in the human glabrous skin area. *The Journal of Physiology*, 232(3):427–452, 1973.

[29] Arun P. Sripati, Sliman J. Bensmaia, and Kenneth O. Johnson. A continuum mechanical model of mechanoreceptive afferent responses to indented spatial patterns. *Journal of Neurophysiology*, 95(6):3852–3864, 2006. PMID: 16481453.

[30] R. W. Van Boven and K. O. Johnson. The limit of tactile spatial resolution in humans. *Neurology*, 44(12):2361–2361, 1994.

[31] R. W. Van Boven, R. H. Hamilton, T. Kauffman, J. P. Keenan, and A. Pascual-Leone. Tactile spatial resolution in blind braille readers. *Neurology*, 54(12):2230–2236, 2000.

[32] J. Tong, O. Mao, and D. Goldreich. Two-point orientation discrimination versus the traditional two-point test for tactile spatial acuity assessment. *Frontiers in Human Neuroscience*, 7:579, 2013.

[33] Vincent Hayward, Alexander V. Terekhov, Sheng-Chao Wong, Pontus Geborek, Fredrik Bengtsson, and Henrik Jörntell. Spatio-temporal skin strain distributions evoke low variability spike responses in cuneate neurons. *Journal of The Royal Society Interface*, 11(93):20131015, 2014.

[34] JR Phillips and KO Johnson. Tactile spatial resolution. III. A continuum mechanics model of skin predicting mechanoreceptor responses to bars, edges, and gratings. *Journal of neurophysiology*, 46(6):1204—1225, December 1981.

[35] Vincent Hayward. Is there a plenhaptic function? *Philosophical Transactions of the Royal Society B: Biological Sciences*, 366(1581):3115–3122, 2011.

[36] Nathan F Lepora, Uriel Martinez-Hernandez, Mathew J. Evans, Lorenzo Natale, Giorgio Metta, and Tony Prescott. Tactile superresolution and biomimetic hyperacuity. *IEEE Transactions on Robotics*, 31(3):605–618, June 2015.

[37] Youcan Yan, Zhe Hu, Zhengbao Yang, Wenzhen Yuan, Chaoyang Song, Jia Pan, and Yajing Shen. Soft magnetic skin for super-resolution tactile sensing with force self-decoupling. *Science Robotics*, 6(51), February 2021. 5.

[38] W. W. Lee, S. L. Kukreja, and N. V. Thakor. Discrimination of dynamic tactile contact by temporally precise event sensing in spiking neuromorphic networks. *Frontiers in Neuroscience*, 11:5, 2017.

[39] S. Bensmaïa. A transduction model of the meissner corpuscle. *Mathematical Biosciences*, 176(2):203 – 217, 2002.

[40] S. S. Kim, S. Sripati, and S. Bensmaïa. Predicting the timing of spikes evoked by tactile stimulation of the hand. *Journal of neurophysiology*, 104:1484–96, 09 2010.

[41] N.A. Macmillan and C.D. Creelman. *Detection Theory: A User's Guide*. Taylor & Francis, 2004.

[42] Joshua Gold and Long Ding. How mechanisms of perceptual decision-making affect the psychometric function. *Progress in neurobiology*, 103, 05 2012.

[43] Lawrence T. DeCarlo. Signal detection models for the same–different task. *Journal of Mathematical Psychology*, 57(1):43–51, 2013.